MODELING PROCESS-DEPENDENT THERMAL SILICON DIOXIDE (SiO_2) FILMS ON SILICON

H.F. Wei [1], A.K. Henning [1], J. Slinkman [2], and J.L. Rogers [2]

[1] Thayer School of Engineering, Dartmouth College, Hanover, NH 03755
[2] IBM General Technology Division, Essex Junction, VT 05452

ABSTRACT

Though extensive work has been done in the Si/SiO_2 system, no process-dependent two-layer SiO_2 film model has ever been established, due largely to the lack of motivation for such a model. This study attempts to model correctly the process dependence of thermal SiO_2 film physical structures and their associated densities, as well as high frequency dielectric constants, so as to provide a foundation for a ULSI process-dependent device reliability simulator. By exploring the characteristic signature of ellipsometric data reduced using a one-layer film model, and comparing it to a two-layer model, we establish a process-dependent, two-layer model for thermal SiO_2 films. Internal consistency in this model is demonstrated using three intrinsic-stress-related phenomena in thermal SiO_2 films on Si. Both the interfacial layer and bulk film are characterized quantitatively for 38 samples, dry-oxidized at four temperatures, leading to three empirical equations describing interlayer thickness, bulk layer density, and bulk layer optical frequency dielectric constant, as functions of oxidation temperature. The interfacial layer refractive index is taken to be independent of oxidation time, and found to be independent of oxidation temperature. The oxidation-temperature-dependent index of refraction of bulk SiO_2 films obtained using the proposed model agrees well with independent one-layer model data on oxides which have thicknesses around the first half-cycle of ellipsometry thickness, for which the interlayer effect is minimal. It is also found that interlayer thickness has a relatively weak dependence on oxidation temperature, which supports the strain energy model for interlayer formation. Application of the thermal SiO_2 film model to Si-device dielectric characterization using fixed index ellipsometry is also discussed, based on recent, new understanding of the ellipsometry equation.

INTRODUCTION

Semiconductor device scaling has followed the set of ideal scaling laws proposed by Dennard and co-workers in 1974 [1], increasing system performance and functionality with higher layout density and lower power-speed product. Projections indicate that by the turn of the century memory and microcomputer chips may have 100 million transistors with 0.2 μm channels and 50 Å gate oxides [2]. On the other hand, chip reliability has improved over the last two decades, driven by customer demand and stiff competition. Projections indicate that by the year 2000 VLSI chips will have failure rates of less than 10 FIT (failure in time) [2]. Both factors have pushed VLSI technologies close to fundamental reliability limits.

One of these limits on device scaling is attributed to hot carrier effects caused by less-than-ideal scaling of power supply voltage. Hot carriers generated in high-field channel regions [3] are emitted into the insulator layers, inducing threshold voltage shifts [4,5]. They are also emitted into the substrate, forming substrate currents which can trigger latchup in CMOS [6]. In deep-submicron MOSFETs, substrate current and gate current are measured at drain biases as

low as 0.7 V and 1.75 V, respectively [7]. While in the '70s and '80s VLSI reliability engineering focus was primarily on predicting system time to failure, today the focus needs to be on understanding the failure mechanisms at the microstructure level, and controlling those process variables which ultimately affect system failure rate [2].

Our broader intent is to create a ULSI process-dependent device reliability simulator, targeted in part for silicon-based devices, to achieve device built-in reliability by using optimal combinations of input process variables. Due to a lack of much fundamental knowledge needed in our proposed simulator, the present work was undertaken to model correctly the physical structures of thermal SiO_2 films and their associated high frequency dielectric constants, as a function of processing temperature. For Si-device gate dielectric thicknesses where the interfacial Si-rich layer (SiO_x, $x<2$) is non-negligible, correct understanding of bulk SiO_2 film and interlayer SiO_x film thicknesses, as well as their respective dielectric constants and densities, is essential for device physics studies. For instance, accurate CV data interpretation, proper account of the image charge potential well at the Si/SiO_2 interface, dielectric breakdown strength analysis, and a-SiO_2 network ring structure statistics, all depend on knowledge of the physical structure of the oxide film throughout its full extent.

EXPERIMENT DESCRIPTIONS

A matrix of 24 device-quality boron-doped (resistivity 11 ~ 16 Ω·cm) <100> 5" silicon wafers was RCA cleaned, then dry-oxidized at several temperatures: 800°C (group I - samples #1 to #8); 900°C (group II - samples #9 to #16); and 1000°C (group III - samples #17 to #24). Wafers were processed at the IBM General Technology Division facility in Essex Junction, VT. The ellipsometric data of a fourth group of samples (denoted as IBM samples #1 to #14) were also used in this study. Most samples in this group (IV) were dry-oxidized at 1050°C on <100> silicon wafers; a few thin oxides were grown at 900°C with 10 minute anneals at 1050°C, as described in [8]. A Rudolph research model 436 manual ellipsometer at the Measurement Standards Lab of IBM Essex Junction was used in this study (operated at wavelength 6328 Å), which is of research grade with polarizer and analyzer resolutions of 0.01°, and specially calibrated [8]. All ellipsometric data were reduced using a recently developed, robust, graphical algorithm [9]. This algorithm uses n-Si = 3.8737 [8] and k-Si = 0.018 for the real and imaginary components of the Si complex refractive index, and n-air = 1.0. We assume all media except the Si substrate are non-absorbing at 6328 Å. The mathematical formulations for the one- and two-layer models used in this work are found in the Appendix. A Digital Instruments NanoScope III AFM was also used to measure the standard deviation of oxide surface roughness.

EXPERIMENTAL RESULTS AND ANALYSIS

Direct evidence of an optically-distinct interlayer between SiO_2 film and Si

Figure 1 shows the oxide thickness-dependent refractive index for the first three groups of samples, assuming a one-layer model (no interfacial layer), as reported previously [10,11, 12,13]. Similar to the error curve technique developed previously [10,11,12], the worst-error curves in Figure 1 were calculated using a one-layer model with refractive index of 1.465 and based on the measurement error combination (Δ, ψ, and angle of incidence) which leads to the largest refractive index deviation from 1.465, as a function of film thickness. Error magnitudes are based on the resolution of the research grade ellipsometer, namely 0.01° for Δ, ψ, and AOI (angle of incidence). Each measurement error for Δ, ψ, and AOI was assigned 3 possible states (−0.01°, 0°, 0.01°). Thus, each pair of points on the worst-error curves was generated after 27 runs of all possible error combinations. It was found that the upper worst-error curve refers to the case where all three measurement errors are negative while the lower worst-error curve refers to the case where all three measurement errors are positive, for oxide thickness less than 970 Å. Neither event is highly probable due to the often random nature of ellipsometric

measurement (Δ and ψ), and AOI error due to laser beam deviation [8]. Data points falling outside the worst-error envelope are considered reliable. The upper error curve in Figure 1 is not completely visible due to the blocking of data points' interpolating lines.

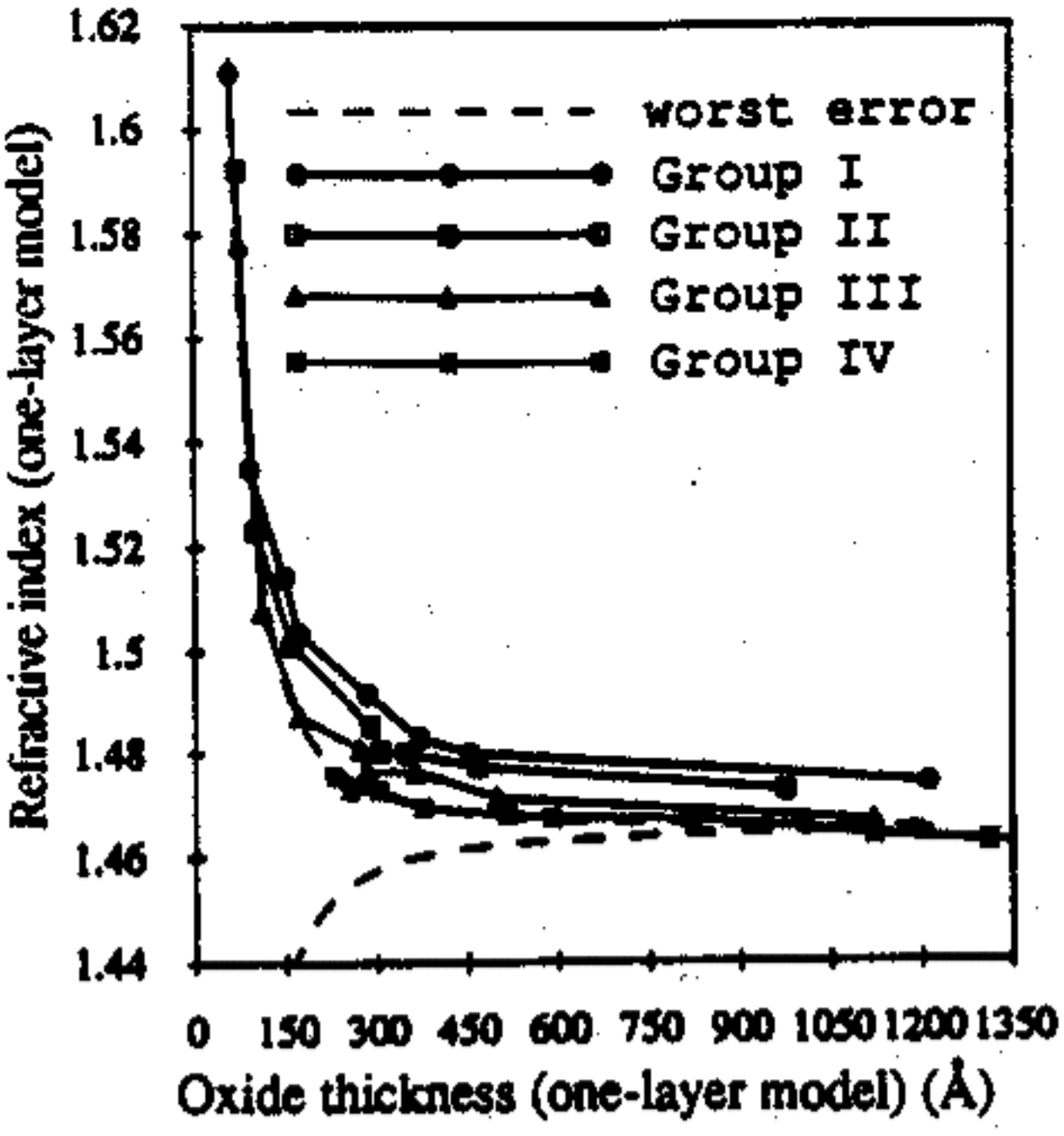

Fig.1 Thickness-dependent refractive index for sample groups I, II, and III.

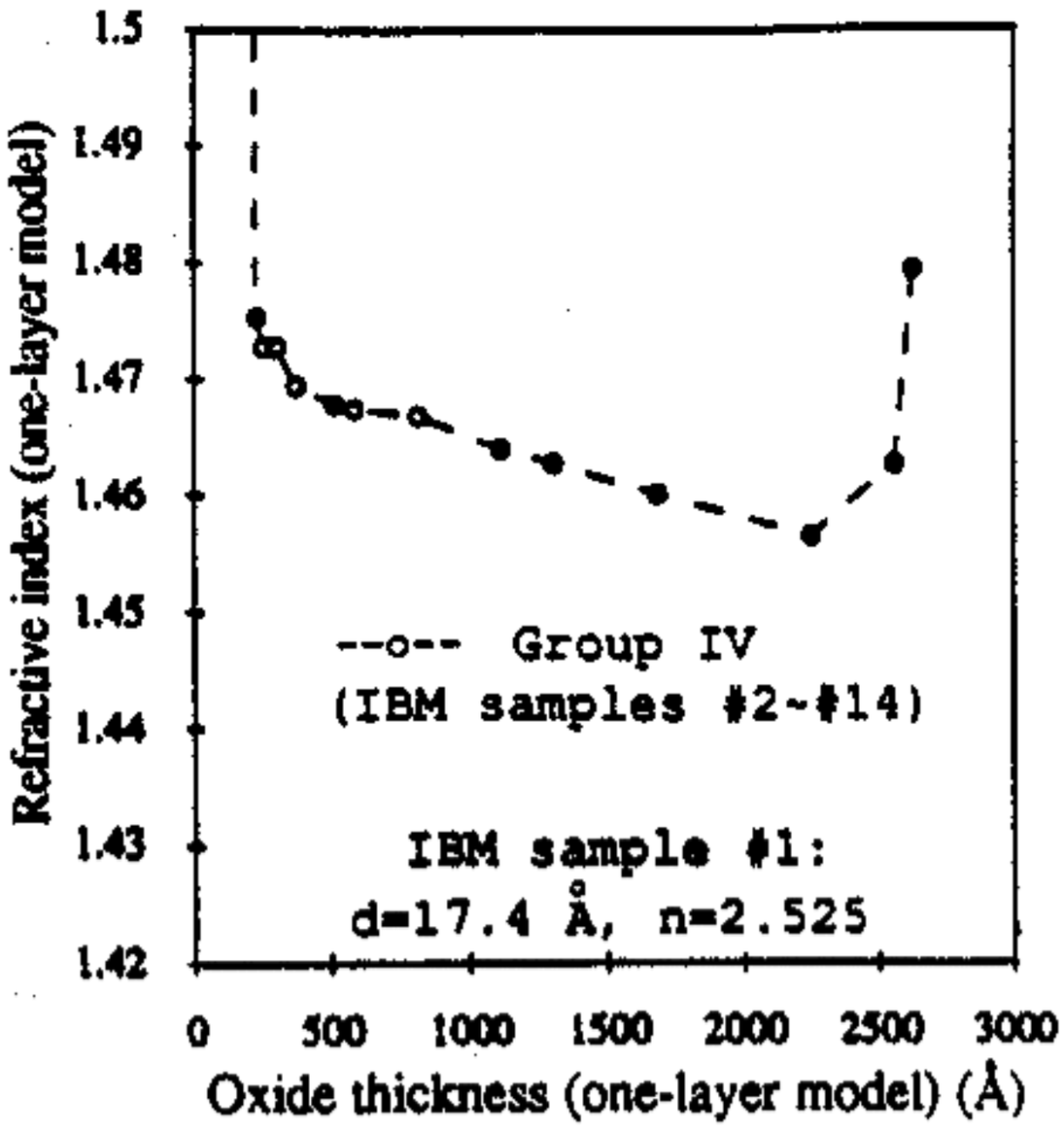

Fig.2 Thickness-dependent refractive index for sample group IV.

Thickness-dependent refractive index based on the one-layer model for the fourth group of samples is shown in Figure 2. The unique "U" shape centered on oxide thickness 1400 Å (half of the first ellipsometric cycle at wavelength 6328 Å) is noteworthy (higher index of refraction near the ellipsometric cycle thicknesses was obtained previously [15]). Note also that the minimum value is less than 1.460, commonly believed to be the index of refraction for fully relaxed thermal a-SiO_2 [14]. Should the oxide have a discrete interlayer of different optical property than that of the bulk oxide film, then a one-layer model interpretation of the actual two-layer structure will estimate film thickness and refractive index incorrectly.

An optically-distinct interlayer creates a unique shape in the graph of relative-error versus film thickness, as shown in the simulation experiment of Figure 3. Here we presume a two-layer structure as suggested previously [15,16], where the interlayer thickness (d_2) is 10 Å with a refractive index of 2.8, and the oxide layer thickness is d_1 with a refractive index of 1.465. The state of polarization (Δ and ψ) was generated as a function of d_1. The one-layer model was used to interpret this state of polarization, which yielded the n_0 (refractive index) and d_0 (thickness) for the hypothetical one-layer oxide. The signature of the interlayer should thus be a "U"-shaped (centered around oxide thickness 1400 Å), thickness-dependent refractive index, with the minimum less than the refractive index for fully-relaxed a-SiO_2 (i.e., 1.460). The data in both Figure 1 (half of the "U" shape) and Figure 2 (the whole "U" shape) reveals the direct evidence of the existence of this optically-different interlayer. Its formation can be attributed to the Si/SiO_2 interface roughness, an off-stoichiometric SiO_x boundary layer [17], and a structurally-distinct region of near-interfacial SiO_2 [17].

Establishment and verification of a two-layer thermal SiO_2 film model

Ideally, any assumptions made in establishing the film model should be based on experimental observations. At the same time, a model based on these assumptions should not lead to predictions which contradict other experimental observations. There are three distinct intrinsic-stress-related phenomena in thermal SiO_2 films on Si [18,19] which lead to assumptions used in our two-layer model:

(1) Intrinsic stress at the Si/SiO_2 interface is oxidation temperature independent;

(2) Intrinsic stress decreases quickly with increasing oxide thickness for oxides grown at the same temperature, finally becoming nearly constant in thick (> 300 Å) oxides;

(3) The magnitude of this constant stress in thick oxides is oxidation-temperature-dependent: the higher the oxidation temperature, the lower this constant stress.

Using index of refraction as an estimator of oxide density and intrinsic stress magnitude, we make the following assumptions:

Assumption I: Based on phenomenon (2) above, we assume the bulk oxide film has the same refractive index (n_1) among samples in each group (notice all samples in this study are grouped according to oxidation temperature). That is, n_1 is oxidation-time-independent at a fixed oxidation temperature;

Assumption II: We further assume both the interlayer index of refraction n_2 and thickness d_2 is also oxidation-time-independent at a fixed oxidation temperature;

Assumption III: For simplicity, we assume both the interlayer and bulk films are uniform; that is, there is no refractive index gradient within each layer.

The d_2 (interlayer thickness) standard deviation, or variance estimator, is examined as a function of n_1 (bulk oxide refractive index) and n_2 (interlayer refractive index) for all four groups of samples. The d_2 variance estimation procedure for a given group of samples is described as follows, using the three assumptions made above:

[i] Fix n_2; [ii] For a given (variable, $1.3 < n_1 < 2$) n_1, calculate d_1 and d_2 for every sample in the group using the ellipsometric data measured with the research grade ellipsometer, then plot the whole sample group d_2 variance estimator versus n_1;

[iii] Repeat steps [i] and [ii] for a different n_2 ($1.3 < n_2 < 4$).

Notice the d_2 variance thus formed for each sample group is a highly non-linear function of n_1 and n_2, using the two-layer model (see Appendix). Based on this procedure, we expect the following outcomes:

A. The value of n_2 obtained should be the same for all 38 samples based on intrinsic-stress phenomenon (1), above;

B. The value of n_1 obtained should be oxidation-temperature-dependent: the higher the oxidation temperature, the lower the n_1, based on intrinsic-stress phenomenon (3);

C. On the plane of n_1 and n_2 which is of physical significance ($1.3 < n_1 < 2$ and $1.3 < n_2 < 4$) the resulting d_2 variance minimum should be unique, and the magnitude of the minimum should not be more than one mono-layer thickness of a-SiO_2 (3.3 Å).

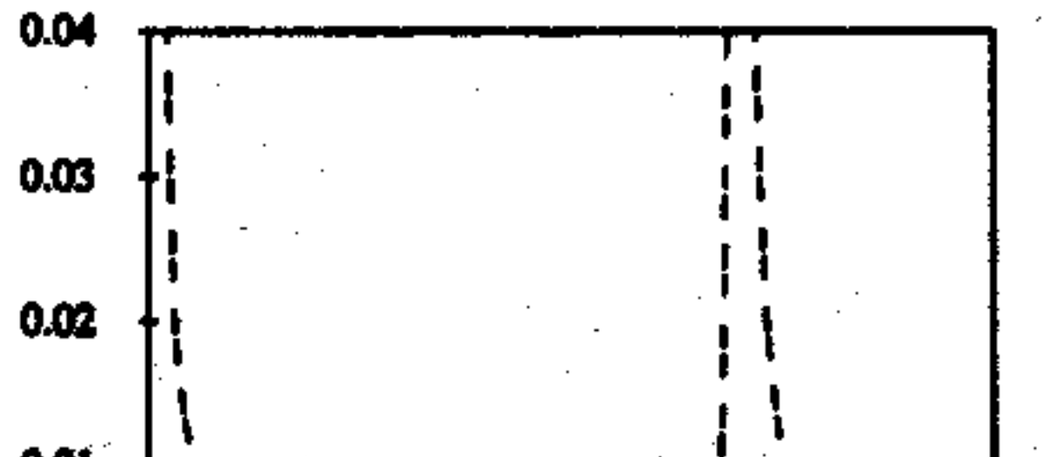

Fig.3 Relative error in refractive index and thickness estimations when a two-layer structure is interpreted by a one-layer model.

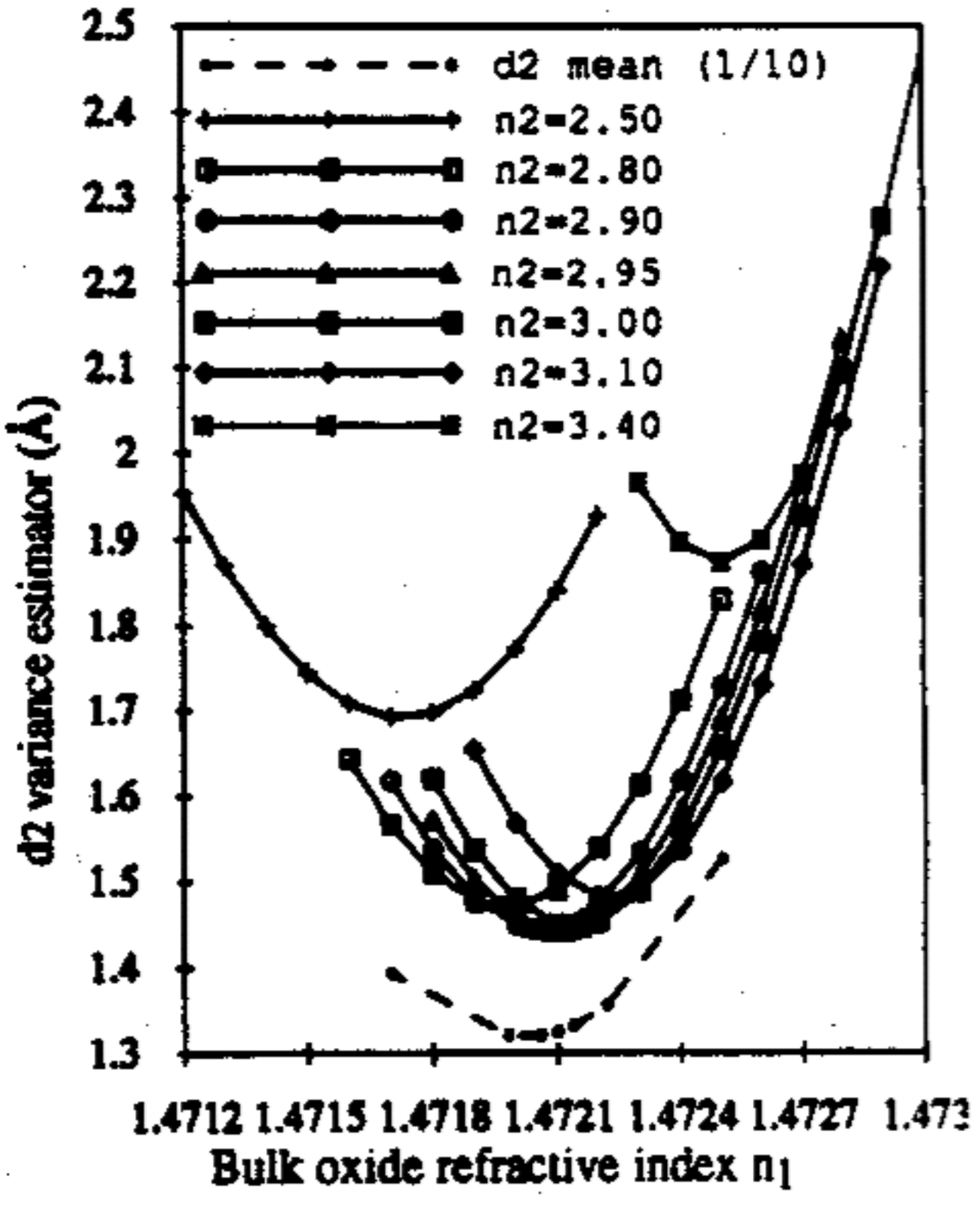

Fig.4 n_2-dependent d_2 variance estimator and d_2 mean (scaled by 10) at the d_2 variance estimation curve minimum for sample group I.

Figure 4 shows the d_2 variance estimation process for group I (800 °C), where only the d_2 variance minimum portion was plotted and the d_2 mean (scaled by 10) was plotted only at the variance estimation curve minimum. Evidently there is a best set of n_1 and n_2 which minimizes the d_2 variance down to 1.45 Å. Thus, the solution of n_1 and n_2 is unique to group I. Incidentally, both d_2 mean and variance are minimized at the same n_1 value. That the d_2 variance minimum (1.45 Å) is less than one mono-layer thickness of a-SiO_2 (3.3 Å) supports Assumption II, that interlayer thickness is essentially the same for sample group I. The d_2 variance minima for the remaining sample groups are found to be between 0.6 Å to 1.4 Å.

The standard deviation of oxide surface roughness of sample #1 was found to be 1.8 Å in a total scanning distance of 8000 Å using the NanoScope III atomic force microscope. It is likely the roughness of the Si-substrate-to-oxide interlayer interface, as well as the interlayer-to-bulk-film interface, are also of the same order (1.8 Å). This may explain why the d_2 variance can not be minimized to zero for any physically significant combination of n_1 and n_2.

Figure 5 shows the d_2 mean for the four groups of samples, using the d_2 standard deviation to mark the upper and lower limit of the error bars. The interlayer refractive index n_2 which minimizes the d_2 standard deviation within each sample group was found to be 2.95 for all four groups of samples. This result is expected based on the growth-temperature-independent interface stress data of [18,19]. Though the d_2 means obtained in this study differ from Taft's reported values at wavelength 5461 Å (d_2 = 7~8 Å for dry 900°C and 4 Å for dry 1200°C, n_2 = 2.8) [15], and Aspnes' reported values at 5461 Å (d_2 = 7±2 Å for dry 1000 °C, n_2 = 3.2±0.5) [16], the d_2 means of this study are close to those found in MOS solar cell open circuit voltage experiments (the oxide non-stoichiometric transition thickness was found to be 13~14 Å) [20].

The relatively weak dependence of interlayer thickness on oxidation temperature in Figure 5 supports the strain energy argument for the interlayer: a large lattice mismatch at the Si/SiO_2 interface can favor an intermediate layer so as to reduce the total free energy, and the interlayer thus formed should be a very slow function of oxidation temperature [21].

Having verified the internal consistency in this two-layer, thermal SiO_2 film model, we turn our attention to the bulk oxide film refractive index (n_1) for the four groups of samples. This was found to be a near-linear function of oxidation temperature, as shown in Figure 6 (n_2 is 2.95). Independent data for thick oxides (1000~1400 Å) based on a one-layer model [22, 23] are also plotted in Figure 6. According to the prediction of Figure 3 (that for oxide thickness around 1400 Å the interlayer effect is a minimum when the one-layer model is used to interpret a two-layer structure), it is expected all these data agree with each other.

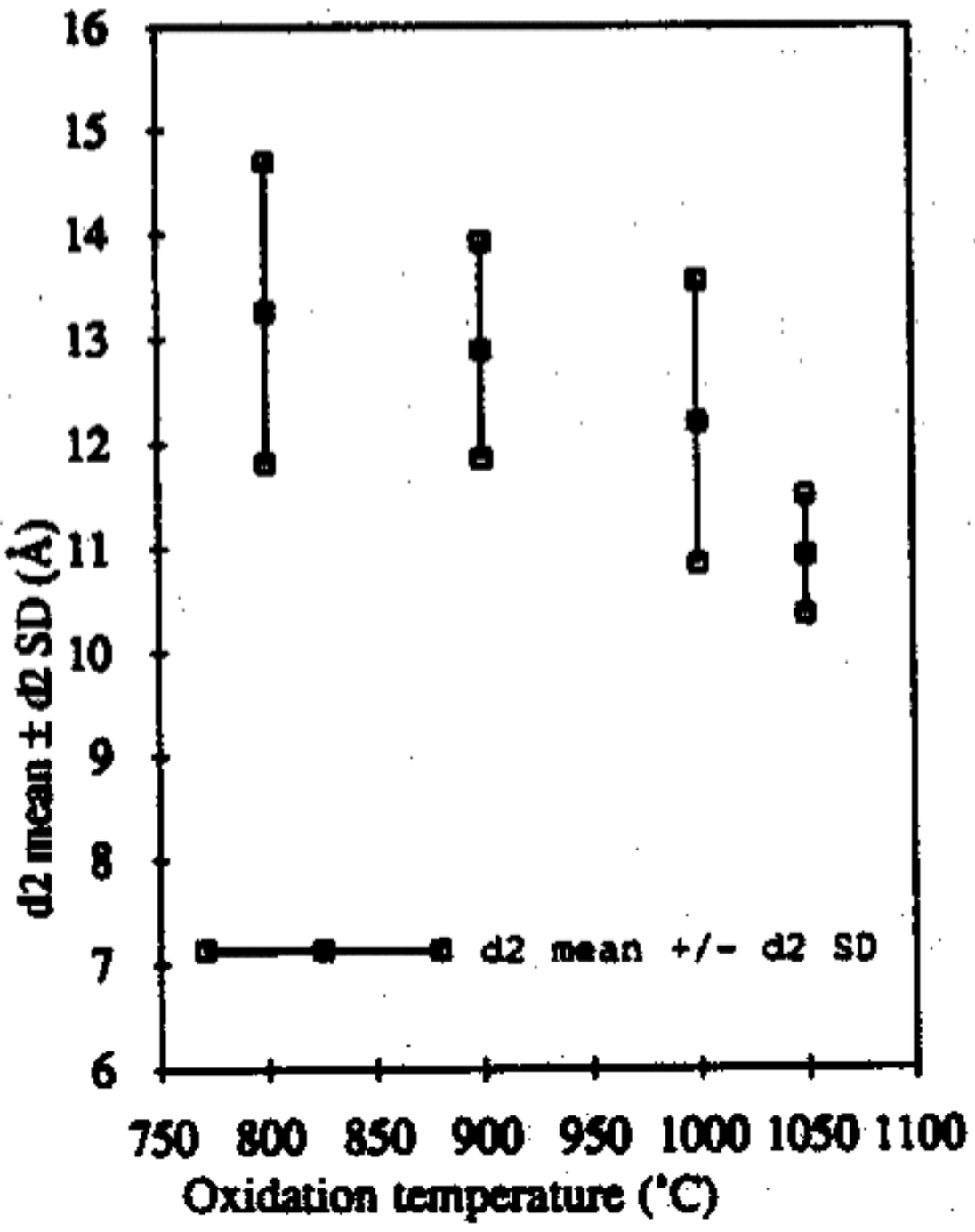

Fig.5 Interlayer thickness d_2 mean ± d_2 standard deviation for all four sample groups.

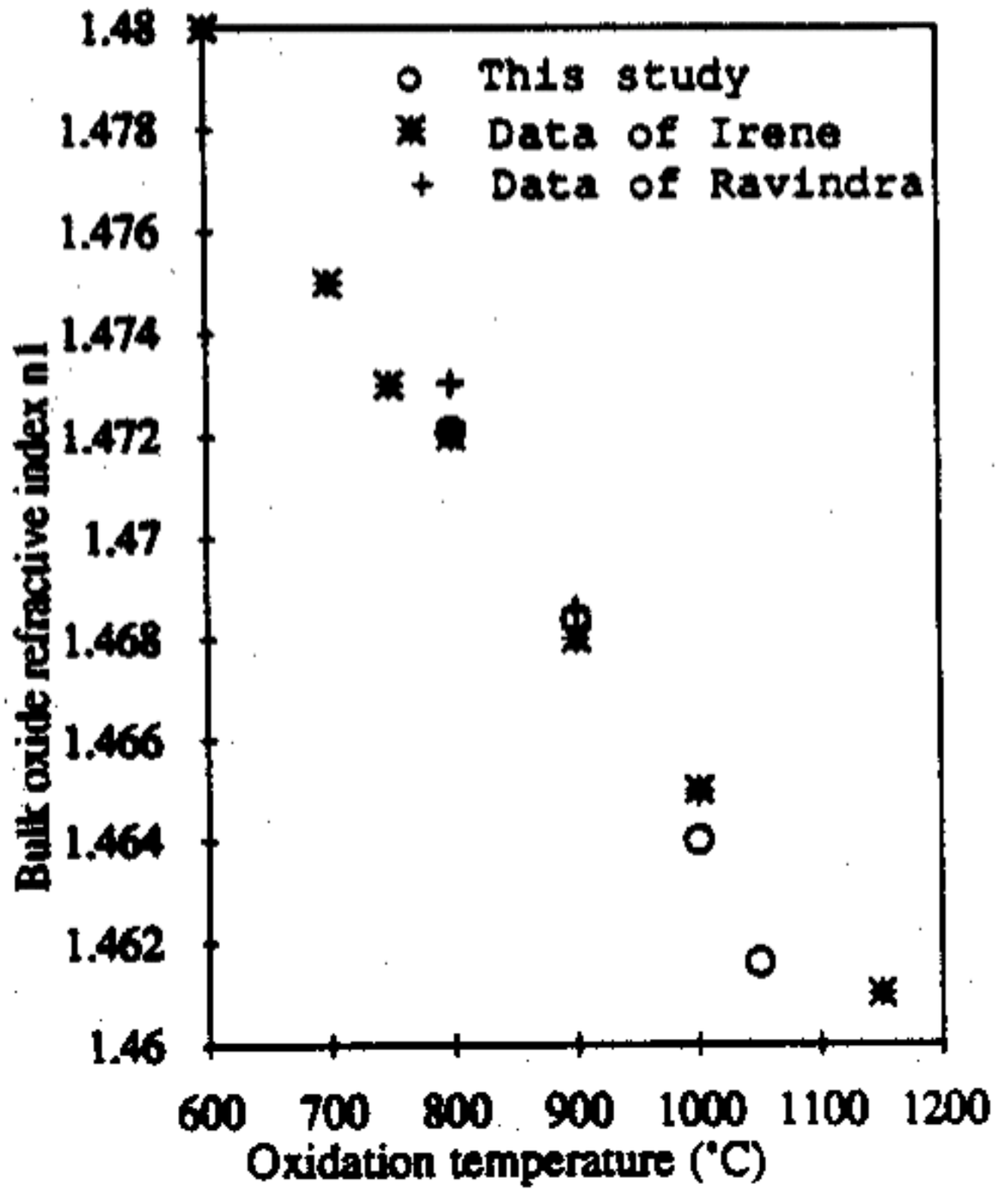

Fig.6 Oxidation-temperature-dependent bulk oxide refractive index n_1 at wavelength 6328 Å.

Further evaluations of the two-layer thermal SiO_2 film model

A simulation experiment in Figure 7 further verifies the validity of the results in Figures 5 and 6 obtained by the technique of d_2 variance estimation. Three sets of thickness-dependent refractive index curves are depicted in Figure 7. Each set consists of three hypothetical two-layer simulations, assuming interlayers of constant thickness (d_2) and refractive index (n_2 = 2.8), and with bulk films of different refractive index n_1. Interlayer thickness differs between the three sets of simulations. The state of polarization (Δ and ψ) is generated as a function of bulk film thickness d_1, using the two-layer model. The one-layer model is then used to interpret this state of polarization in terms of the thickness-dependent refractive index curves plotted in Figure 7, similar to the procedure used in Figure 3. The simulation curves using different n_2 (varied from 2.6 to 3.0) show little shift from those in Figure 7, compared with the effects caused by d_2 changes. However, the state of polarization (Δ and ψ) generated using a two-layer model in which n_2 is varied from 2.6 to 3.0, does indicate shifts though much smaller than that caused by the d_2 changes, but large enough (more than 0.01°) to be detected. Thus, the range of n_2 (2.8±0.2) should not be interpreted as an uncertainty range.

Four features can be generalized from Figure 7:

(1) The thickness-dependent refractive index (two-layer structure interpreted by a one-layer model) is relatively insensitive to interlayer refractive index n_2 (compared to its sensitivity to d_2 and n_1), for the range $n_2 = 2.6 \sim 3.0$ and the axis scale used in Figure 7;

(2) Differences in bulk film refractive index n_1 cause marked distinctions in the thickness-dependent refractive index curves using the one-layer model interpretation;

(3) All thickness-dependent refractive index curves merge together for oxides thinner than 150 Å, should the two-layer structures these curves represent have the same interfacial layer (n_2, d_2), but different n_1;

(4) For oxide thickness less than 150 Å, the thickness-dependent refractive index curves are distinct only when the two-layer structures these curves represent have interfacial layer (d_2) thicknesses differing by more than around one mono-layer of a-SiO_2.

The relative insensitivity of the d_2 variance estimator and the minimum of n_1 versus n_2 found in Figure 4, agree with feature (1). According to feature (2), distinctions for oxides thicker than 150 Å in Figure 1 imply each sample group should have a distinct bulk film refractive index n_1. Based on features (3) and (4), the convergent behavior for oxide thickness less than 150 Å in Figure 1 implies the interlayer thickness should not differ by more than one a-SiO_2 monolayer for all 38 samples studied. Both conclusions agree with the experimental results in Figures 5 and 6.

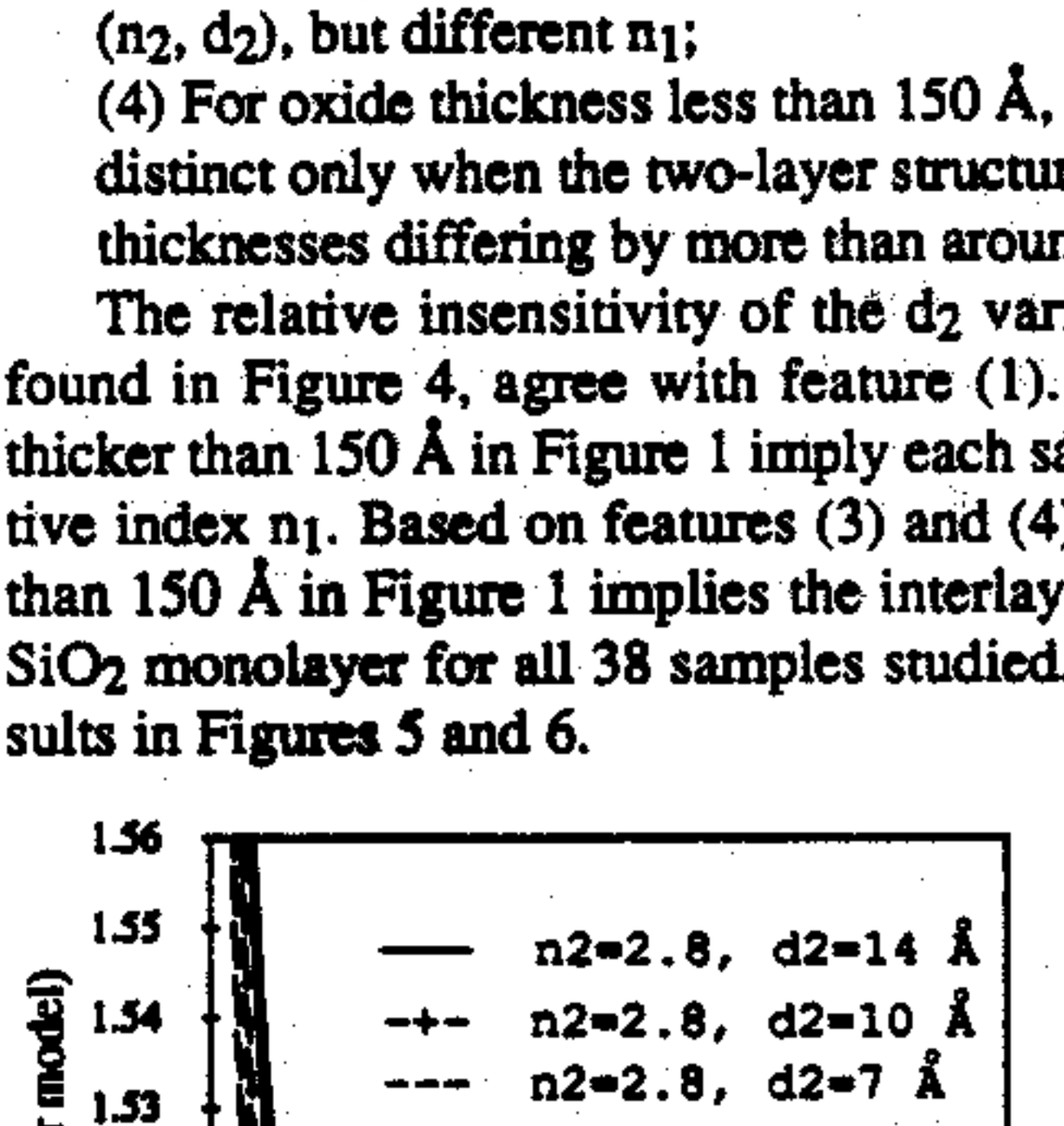

Fig.7 Thickness-dependent refractive index for three sets of hypothetical two-layer structures as interpreted by a one-layer model.

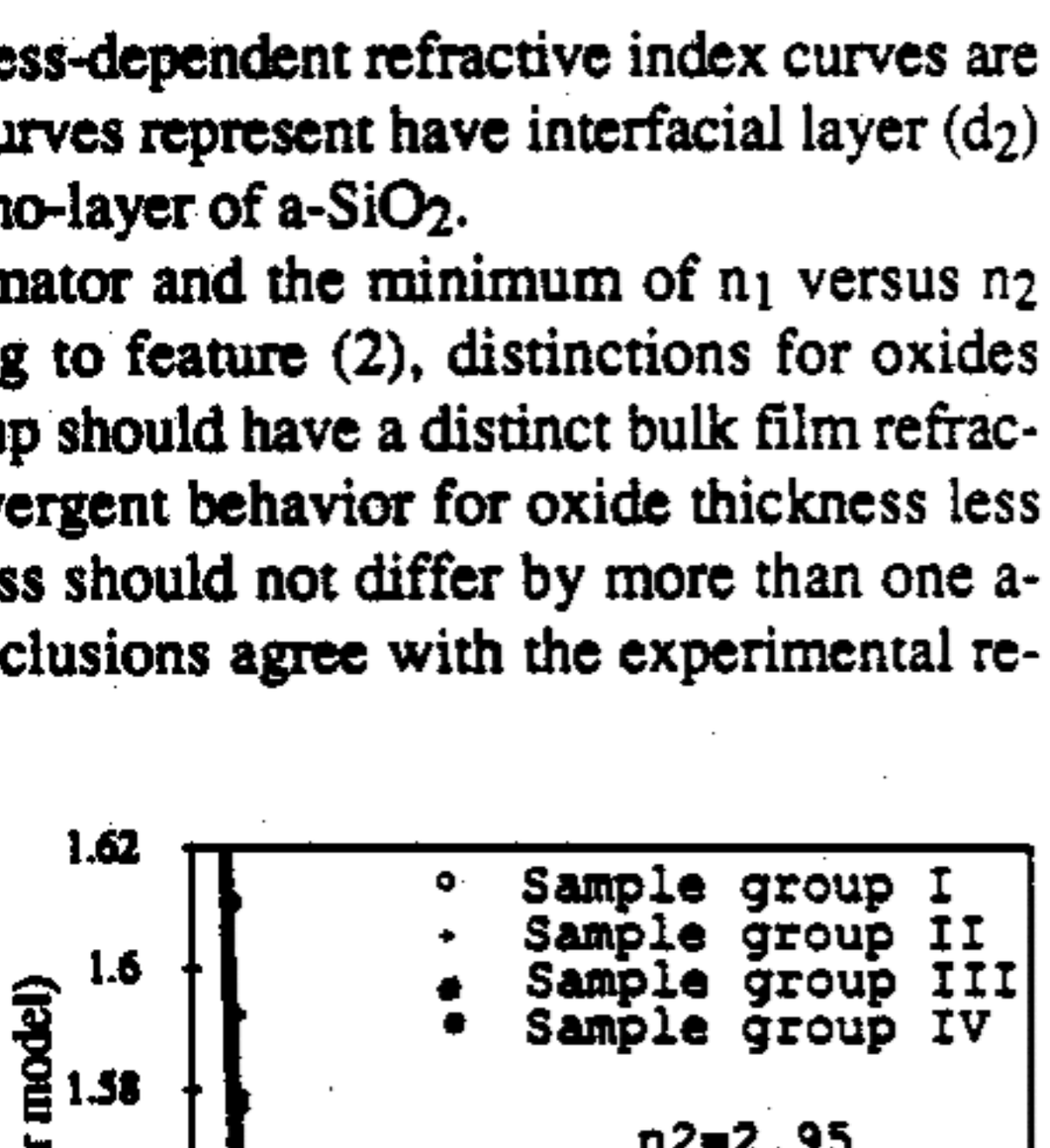

Fig.8 Thickness-dependent refractive index simulations of two-layer structures as interpreted by a one-layer model, compared with Fig. 1.

Consequently, we compare thickness-dependent refractive index simulations of two-layer structures as interpreted by a one-layer model, with the experimental curves of Figure 1, as shown in Figure 8 (the values of n_2, d_2, and n_1 used in the simulations are from results of Figures 5 and 6). Note that the simulations in Figure 8 are NOT obtained by direct fitting of the experimental curves of Figure 1. Instead, they are obtained using the d_2 variance estimations as shown in Figure 4. The fine match between simulations and experimental curves shown in Figure 8 in turn supports the validity of the d_2 variance estimation procedure using the assumptions inherent in the two-layer thermal SiO_2 film model.

It is worth noting that we have assumed the interlayer is also non-absorbing at 6328 Å in our ellipsometric data reductions. The assumption that $k_2 \approx 0$ is indeed a valid one, since by setting $k_2 = 0.009$ (half of the extinction coefficient of Si at 6328 Å) in the ellipsometric program using the n_2, d_1, d_2, and n_1 ranges in this study, the change in the state of polarization (Δ and ψ) generated is less than 0.01° in most cases, which is beyond the resolution of the research grade ellipsometer used.

Empirical equations in the two-layer thermal SiO_2 film model

Fitting the data of Figure 5 yields the following empirical equation for interlayer thickness d_2 (Å) as a function of oxidation temperature T (°C):

$$d_2 = -11.035 + 6.1146 \times 10^{-2}\,T - 3.8181 \times 10^{-5}\,T^2 \qquad (1)$$

Film density can be extracted from the refractive index, using the Lorentz-Lorenz relation given by:

$$\left[\frac{n^2 - 1}{n^2 + 2}\right] \frac{M}{\rho} = \frac{4\pi}{3} N\alpha \qquad (2)$$

where n is the index of refraction, M is the molecular weight, ρ is the mass density, and N is Avogadro's number. α is the total polarizability of the molecule, with $\alpha = \alpha_e$ (electron polarizability) $= 2.95 \times 10^{-24}$ cm^3 [23]. Using this expression, bulk film density ρ (g/cm^3) was calculated as shown in Figure 9. In the absence of specific composition data for the interlayer, calculation of its density is not possible.

In a nonferromagnetic ($\mu_r = 1$) and insulating ($\sigma \approx 0$) material such as a-SiO_2, the relationship between high frequency relative complex dielectric constant and complex refractive index is given by [24]:

$$\varepsilon_1 - i\,\varepsilon_2 = (n - ik)^2 \qquad (3)$$

The real part of the relative complex dielectric constant is also shown in Figure 9 (with interlayer relative dielectric constant $\varepsilon_1 = 8.7025$), assuming the extinction coefficient k for both the bulk film and interlayer is negligible at 6328 Å.

Fitting the data of Figure 9 yields the following two empirical equations for bulk film density (g/cm^3) and high frequency dielectric constant as functions of oxidation temperature T (°C):

$$\rho = 2.4 - 1.7309 \times 10^{-4}\,T \qquad (4)$$

$$\varepsilon_1 = 2.2662 - 1.2322 \times 10^{-4}\,T \qquad (5)$$

Due to their empirical nature, the validity of these expressions outside the temperature range studied (800°C ~ 1050°C) is not assured.

APPLICATION OF THE SiO_2 FILM MODEL TO Si-DEVICE DIELECTRIC CHARACTERIZATION USING FIXED INDEX ELLIPSOMETRY

Our recent studies on the ellipsometry equation found that the imaginary part of the ellipsometry equation has an impressive resistance to common measurement errors. They concluded that, if it is necessary to fix refractive index to obtain the thin SiO_2 film thickness

from the ellipsometry equation, using either one- or two-layer film models, then the imaginary part of the ellipsometry equation should be used [9]. Since in a production environment the commonly used ellipsometers have polarizer and analyzer resolutions of around 0.1°, the refractive index must be fixed in the ellipsometric data reduction for measuring oxide films thinner than ~70 Å in order to obtain a physical solution from the ellipsometry equation [9]. The thermal SiO_2 film model developed in this work can be readily used to predict, at a specific oxidation temperature, the value of the bulk film refractive index which should be used, and the optical interference due to the interlayer. Thus the solution of the imaginary part of the ellipsometry equation using our film model predictions will be much closer to the actual oxide thickness, given the precision of the ellipsometric data. This should ensure greater control of Si-device dielectric thickness specifications in manufacturing. It also provides guidelines for Si oxidation model development in the initial thin oxide regime, since most oxide growth data with which oxidation models have been compared were obtained using fixed-index ellipsometry.

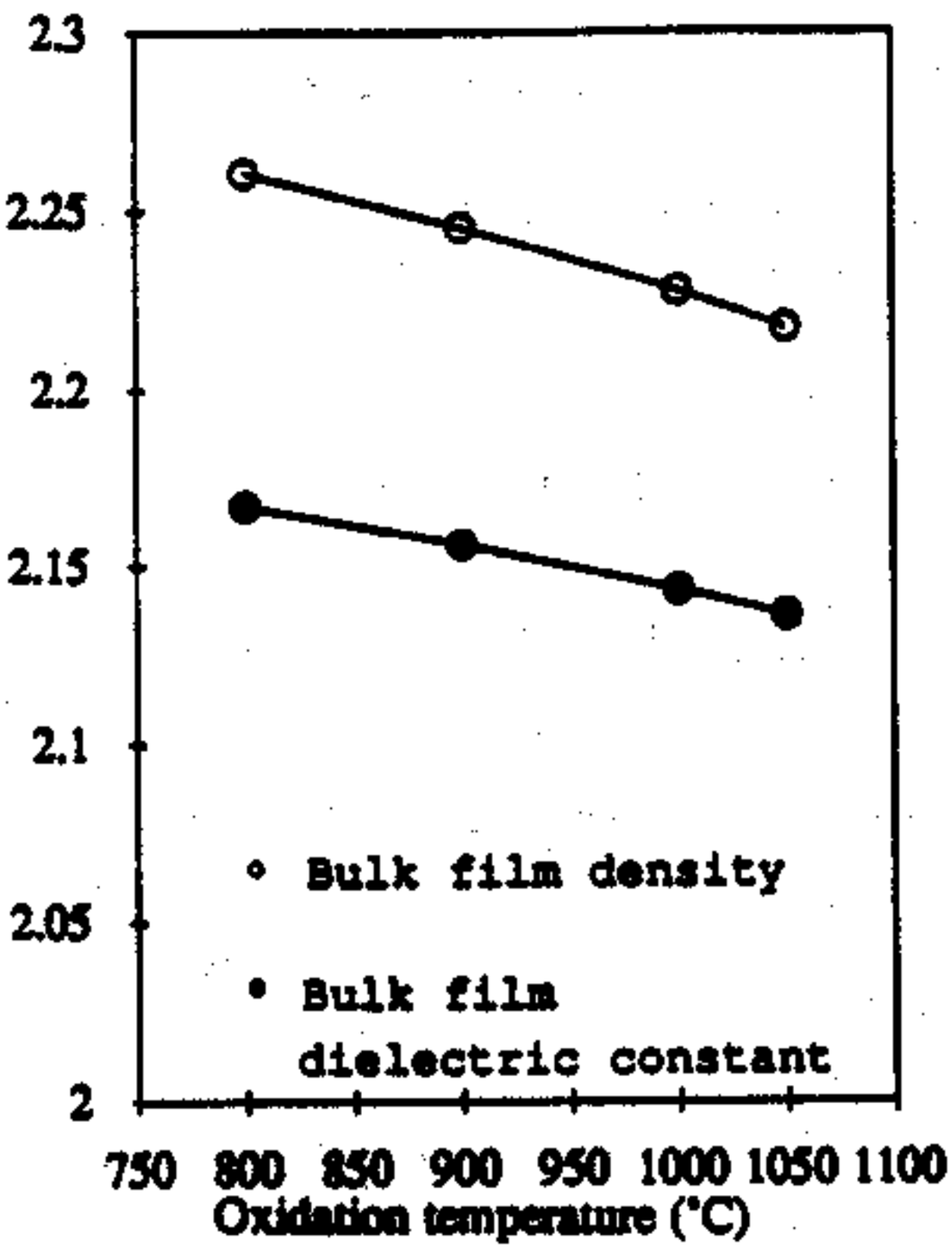

Fig.9 Oxidation-temperature-dependent bulk film density (g/cm^3) and optical frequency ε_1 (with the interlayer ε_1=8.7025).

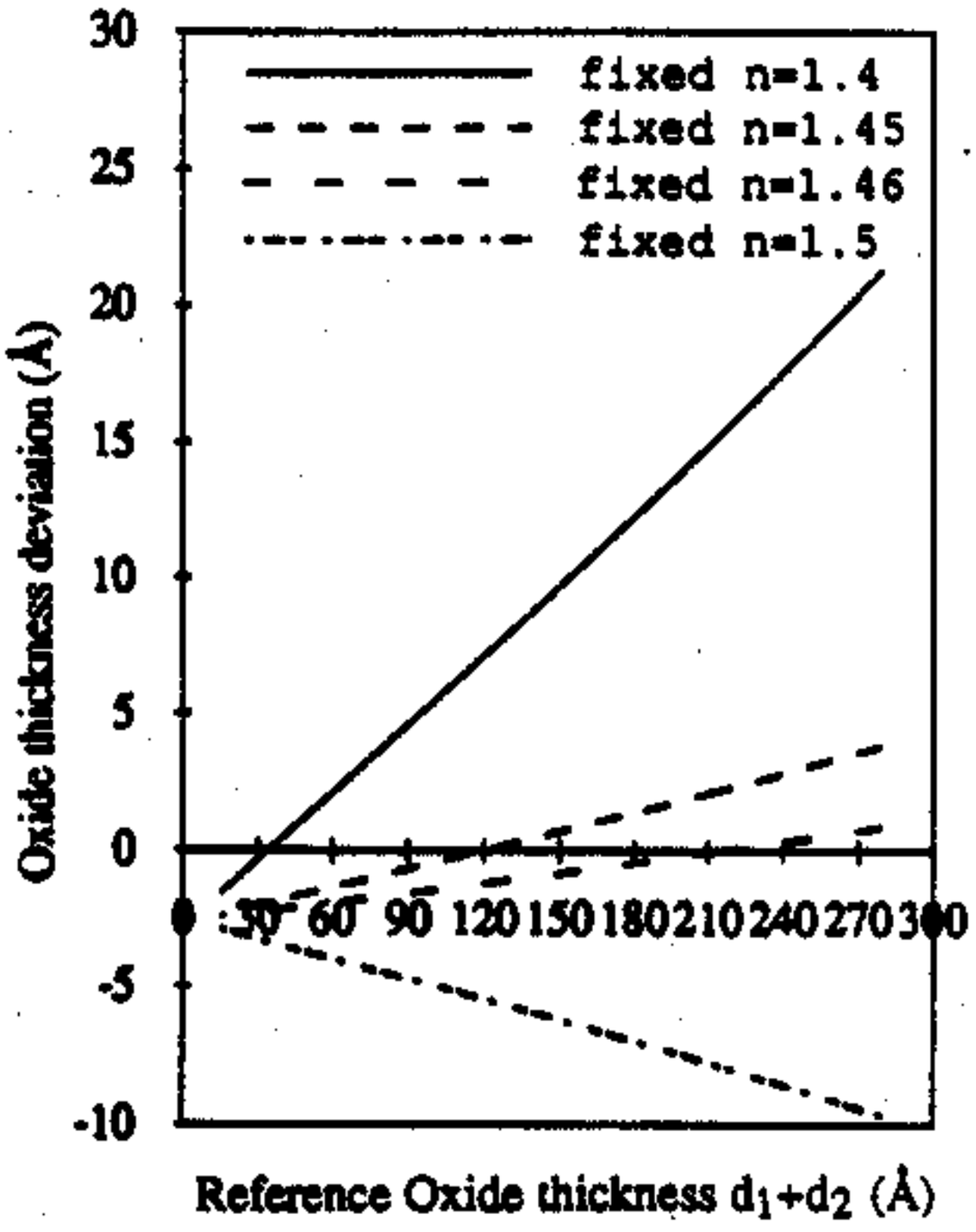

Fig.10 Oxide thickness deviations due to one-layer model, fixed index, ellipsometric interpretations of oxides dry grown at 800 °C.

The simulation experiment in Figure 10 indicates the error of oxide thickness introduced by the one-layer model, fixed-index ellipsometry. Here we treat the two-layer SiO_2 film model as the reference. The state of polarization (Δ and ψ) was generated as a function of total oxide thickness, using $n_2 = 2.95$, $d_2 = 13.3$ Å, $n_1 = 1.4721$ (results obtained in Figure 4 for 800°C), and various d_1 (bulk film thickness). The one-layer model, fixed-index ellipsometry program associated with a commercial ellipsometer was used to interpret this state of polarization (data input to the fifth digit after decimal) to obtain oxide thickness. The oxide thickness deviations from the reference are plotted in Figure 10. The thickness deviation in this figure is solely caused by differences in SiO_2 film models, since the effect of ellipsometric measurement error is not accounted for in the simulation experiment.

SUMMARY

The interplay between experimental observations and two-layer oxide optical analysis leads to the identification of an optically different interfacial layer, as suggested previously [15,16]. Both the interlayer and bulk film are characterized quantitatively for 38 samples, dry-oxidized at

four temperatures, based on assumptions supported by measured stress data [18,19]. The self-consistent, process-dependent, two-layer, thermal SiO_2 film model is established and can be summarized as follows:

(1) Thermal SiO_2 films on Si are well-described using a discrete, two-layer model, consisting of a bulk film and an interfacial layer;

(2) The interlayer thickness is in the range of 11 ~ 13 Å, and a weak function of the oxidation temperature in the range 800°C ~ 1050°C. It is independent of oxidation time;

(3) The interlayer refractive index is 2.95, independent of oxidation temperature and time;

(4) Bulk film refractive index is a near-linear function of oxidation temperature.

Three empirical equations were generated to describe interlayer thickness, bulk layer density, and bulk layer optical frequency dielectric constant as functions of oxidation temperature. Application of the thermal SiO_2 film model to Si-device dielectric characterization using fixed-index ellipsometry is also discussed. The self-consistent, process-dependent, two-layer, thermal SiO_2 film model established in this study is a key constituent in formulating a ULSI process-dependent device reliability simulator.

APPENDIX

The ellipsometry equation is expressed as [25]:

$$\tan(\psi)\exp(i\Delta) = \frac{R_p}{R_s} \tag{1}$$

where Δ and ψ describe the state of polarization of reflected light, and R_p and R_s are the total Fresnel reflection coefficients at the film surface for p- and s-polarized monochromatic light. The particular expressions for R_p and R_s are film-model-dependent (e.g., one- or two-layer model, models incorporating stress-optic effect or optical anisotropy). The equations leading to the final expressions of R_p and R_s are as follows for the one-layer model [25]:

$$r_{s,i} = \frac{N_{i-1}\cos\theta_{i-1} - N_i\cos\theta_i}{N_{i-1}\cos\theta_{i-1} + N_i\cos\theta_i} \quad (2), \qquad r_{p,i} = \frac{N_i\cos\theta_{i-1} - N_{i-1}\cos\theta_i}{N_i\cos\theta_{i-1} + N_{i-1}\cos\theta_i} \tag{3}$$

$$\alpha = \frac{4\pi d}{\lambda}\sqrt{N_1^2 - N_0^2\sin^2\theta_0} \quad (4), \qquad N_0\sin\theta_0 = N_1\sin\theta_1 = N_2\sin\theta_2 \tag{5}$$

$$R_S = \frac{r_{s,1} + r_{s,2}\cdot e^{-i\alpha}}{1 + r_{s,1}\cdot r_{s,2}\cdot e^{-i\alpha}} \quad (6), \qquad R_p = \frac{r_{p,1} + r_{p,2}\cdot e^{-i\alpha}}{1 + r_{p,1}\cdot r_{p,2}\cdot e^{-i\alpha}} \tag{7}$$

where $r_{s,i}$ and $r_{p,i}$ are the Fresnel reflection coefficients at the i-th interface for s- and p-polarized light (the ambient-to-film interface corresponds to i = 1; the film-to-substrate interface corresponds to i = 2); N_0, N_1, and N_2 are complex refractive indexes for the ambient (air), film, and the substrate ($N = n - ik$, where n is index of refraction [the real part of N] and k is the extinction coefficient [the imaginary part of N]); θ_0 is the angle of incidence at the first interface (ambient/film), θ_1 and θ_2 are angles of refraction; α is the phase factor in the film for s- or p-polarized light, d is the film thickness, λ is the wave length. Equation (5) is Snell's law.

For the two-layer film model, along with equations (1), (2), and (3), the following equations are also coupled [25]:

$$\alpha_1 = \frac{2\pi d_1}{\lambda}\sqrt{N_1^2 - N_0^2\sin^2\theta_0} \quad (8), \qquad \alpha_2 = \frac{2\pi d_2}{\lambda}\sqrt{N_2^2 - N_1^2\sin^2\theta_1} \tag{9}$$

$$N_0\sin\theta_0 = N_1\sin\theta_1 = N_2\sin\theta_2 = N_3\sin\theta_3 \tag{10}$$

$$R_S = \frac{r_{s,1} + r_{s,2}\,e^{-2i\alpha_1} + r_{s,3}\,e^{-2i(\alpha_1+\alpha_2)} + r_{s,1}\,r_{s,2}\,r_{s,3}\,e^{-2i\alpha_2}}{1 + r_{s,1}\,r_{s,2}\,e^{-2i\alpha_1} + r_{s,1}\,r_{s,3}\,e^{-2i(\alpha_1+\alpha_2)} + r_{s,2}\,r_{s,3}\,e^{-2i\alpha_2}} \tag{11}$$

$$R_p = \frac{r_{p,1} + r_{p,2}\, e^{-2i\alpha_1} + r_{p,3}\, e^{-2i(\alpha_1+\alpha_2)} + r_{p,1}\, r_{p,2}\, r_{p,3}\, e^{-2i\alpha_2}}{1 + r_{p,1}\, r_{p,2}\, e^{-2i\alpha_1} + r_{p,1}\, r_{p,3}\, e^{-2i(\alpha_1+\alpha_2)} + r_{p,2}\, r_{p,3}\, e^{-2i\alpha_2}} \qquad (12)$$

where $r_{s,i}$ or $r_{p,i}$ is the Fresnel reflection coefficient at the ith interface for s- or p-polarized light (the ambient-to-film interface corresponds to i = 1; the bulk-film-to-interlayer interface corresponds to i = 2; the interlayer-to-substrate interface corresponds to i = 3); N_0, N_1, N_2, and N_3 are complex refractive indexes for the ambient (air), bulk film, interlayer, and the substrate; θ_0 is the angle of incidence at the first interface (ambient/bulk-film), θ_1, θ_2, and θ_3 are angles of refraction; α_1 and α_2 are the phase factors in the bulk film and interlayer respectively, for s- or p-polarized light. d_1 and d_2 are thicknesses of the bulk film and interlayer.

ACKNOWLEDGEMENTS

The authors thank D. Baker of IBM GTD Essex Junction for wafer oxidation preparations. This work was supported by an IBM-Shared University Research Grant through the IBM GTD, Essex Junction, VT 05452-4299.

REFERENCES

[1] R.H. Dennard, F.H. Gaensslen, H.N. Yu, V.L. Rideout, E. Bassous, and A.R. LeBlanc, *IEEE J Solid-State Circuits* **SC-9**(5):256, 1974.
[2] D.L. Crook, **28th** IRPS/IEEE, p.2, 1990.
[3] A.K. Henning, "Hot Carrier Effects in CMOS Field Effect Transistors at Cryogenic Temperatures," Ph.D. dissertation, Stanford University, 1987.
[4] D.M. Erb, H.G. Dill, and T.N. Toombs, *IEEE Trans Elec Dev* **ED-18**:105, 1971.
[5] T.H. Ning, *Solid-State Electronics* **21**(1):273, 1978.
[6] C.M. Wang, J.J. Tzou, and C.Y. Yang, **27th** IRPS/IEEE, p.110, 1989.
[7] J. Chung, M.C. Jeng, J.E. Moon, P.K. Ko, and C.Hu, **27th** IRPS/IEEE, p.92, 1989.
[8] J.C. Panner, E.W. Conrad, and J.L. Rogers, *Thin Solid Films* **206**(1-2):381, 1991.
[9] H.F. Wei, A.K. Henning, J. Slinkman, and W.R. Hunter, *J Electrochem Soc* **139**(6):1783, 1992.
[10] J.H. Ho, C.L. Lee, C.W. Jen, and T.F. Lei, *Solid-State Electronics* **330**(9):973, 1987.
[11] A. Kalnitsky, S.P. Tay, J.P. Ellul, S. Chongsawangvirod, J.W. Andrews, and E.A. Irene, *J Electrochem Soc* **137**(1):234, 1990.
[12] S. Chongsawangvirod, E.A. Irene, A. Kalnitsky, S.P. Tay, and J.P. Ellul, *J Electrochem Soc* **137**(11):3536, 1990.
[13] T.S. Chao, C.L. Lee, and T.F. Lei, *J Electrochem Soc* **138**(6):1756, 1991.
[14] L.M. Landsberger and W.A. Tiller, *Appl Phys Lett* **51**(18):1416, 1987.
[15] E. Taft and L. Cordes, *J Electrochem Soc* **126**(1):131, 1979.
[16] D.E. Aspnes and J.B. Theeten, *J Electrochem Soc* **127**(6):1359, 1980.
[17] F.J. Grunthaner and P.J. Grunthaner, *Mater Sci Repts* **1**(2-3):65, 1986.
[18] G. Lucovsky, J.T. Fitch, E. Kobeda, and E.A. Irene, in "The Physics and Chemistry of SiO_2 and the Si-SiO_2 Interface," eds. C. R. Helms and B. E. Deal (Plenum, New York, 1988), p. 139.
[19] E. Kobeda and E.A. Irene, *J Vac Sci Technol* **B6**:574, 1988.
[20] R. Singh, K. Rajkanan, and J. Shewchun, in "Physics of SiO_2 and its Interfaces," ed. S.T. Pantelides (Pergamon, New York, 1978), p. 396.
[21] N.F. Mott, S. Rigo, F. Rochet, and A.M. Stoneham, *Phil Mag B*, **60**(2):189, 1989.
[22] E.A. Irene, E. Tierney, and J. Angilello, *J Electrochem Soc* **129**(11):2594, 1982.
[23] N.M. Ravindra, J. Narayan, D. Fathy, J.K. Srivastava, and E.A. Irene, *J Mater Res* **2**(2):216, 1987.
[24] R.H. Bube, "Electrons in Solids" (Academic Press, New York, 1981).
[25] R.M.A. Azzam and N.M. Bashara, "Ellipsometry and Polarized Light" (North-Holland, Amsterdam, 1977).